JOURNAL OF MATERIALS SCIENCE **33** (1998) 5883–5890

Shock-induced phase transitions among SiC polytypes

Y. Q. ZHU, T. SEKINE*, T. KOBAYASHI, E. TAKAZAWA
National Institute for Research in Inorganic Materials, Namiki 1-1, Tsukuba, Ibaraki 305-0044, Japan
E-mail: sekine@nirim.go.jp

A series of recovery experiments was conducted using a propellant single-stage gun on starting materials of both α-SiC and β-SiC. X-ray examination on the recovered samples indicated that obvious polytype transformations among 3C, 6H, and 15R took place. To the α-SiC starting material, 15R tends to increase and 6H tends to decrease, while a small amount of α-SiC form transforms to 3C type, along with increasing the shock temperature and pressure. X-ray diffraction analysis showed that the β-SiC polytype is transformed into rhombohedral forms. From results of both types of SiC samples, rhombohedral polytypes seem to be the favored shock modification. The effects of shock pressure and shock temperature and their heterogeneous distribution on these polytype transitions are discussed in detail. Analysis showed that these polytype transitions resulted from the stacking sequence changes of SiC atom layers.

1. Introduction

The recent growing scientific and technological interest in silicon carbide (SiC) arises from its significant physical, mechanical, and chemical properties and its high thermal stability [1], which is driven by the existence of a variety of different polytypes of SiC. About 200 crystallographic modifications have been reported so far [2]. This outstanding behavior makes it useful for electronic or optical uses, which can be applied in high-power, high-speed, high-temperature, and high-frequency devices, for example. The most favorable polytype for a device application is still in debate. The polytypism originates from differences in stacking sequence of Si–C bilayers along the [1 1 1] or [0 0 0 1] direction, giving rise to cubic (C), hexagonal (H), or rhombohedral (R) arrangements of *n* double layers within a unit cell. The most common polytypes are believed to be 3C (zinc blend type, β-type SiC) and 6H, 4H, and 15R in the classifications of α-type SiC, although the long-period polytype of SiC, 51R, had been reported as being very stable at higher temperatures [3].

In the last several decades, the polytype transformation of SiC has been studied in various physical and chemical conditions: i.e., at temperatures of 1200–2600 °C [4, 5], at high pressures [6–8], and impurities contained in raw materials [9]. Fig. 1 is a summary of the relationship between temperature and preferred polytype structures of SiC. It shows that 6H is the favored form at high temperatures and 3C is a low-temperature form or metastable form only. On the other hand, the recent development of the diamond anvil cell and related examination techniques used in the ultra-high pressure ($\sim$ 100 GPa) study enables us to investigate the high-pressure phase occurrence or phase transition under ambient temperature. Fruitful results have also been obtained for SiC [10, 11]. Moreover, an experimental study proved that 6H polytype remained stable up to 95 GPa while 3C polytype changed from zinc blend structure to rock-salt structure at about 100 GPa [11]. However, the study under both high-temperature and high-pressure conditions has been rarely reported due to instrument limitations. Shock wave compression employed in the study of SiC, however, was limited to be only a means of consolidifying the powders aiming to obtain high-density bulk ceramic materials [13], which might be due to two reasons. The first is higher defect densities in post-shock samples by shock wave or shear stress, such as dislocations and stacking defaults, which makes it difficult to obtain a well-crystallized structure. The second is that even with well-crystallized single-crystal SiC, the quantitative analysis of a mixture of different modifications by the X-ray diffraction (XRD) method has posed a technical problem for a long time, due to its overlapping or coinciding peaks in the diffraction pattern.

Until now, a few methods in SiC polymorph determination have been established [14–16]. In this study, we apply the simplest and the most convenient method established by Ruska *et al.* [15], which is to calculate the polytype contents based on the intensities of some typical diffraction peaks.

In the present research, by using a single-stage propellant gun, a series of shock-recovery experiments on high-purity SiC starting materials (α- and β-SiC)

* Author to whom all correspondences should be addressed.

TABLE I Chemical composition of the starting materials

α-SiC (wt %)		β-SiC (wt %)	
SiC content	99%	SiC content	97.35∼98.36%
Free carbon	0.55%	Free carbon	2.34∼3.04%
Free SiO_2	0.33%	Total nitrogen	<0.03%
Fe	0.034%	Total metal	<2 PPm
Al	0.011%	Particle shape:	Nearly sphere
Particle size	∼400 nm	Particle size	∼30 nm

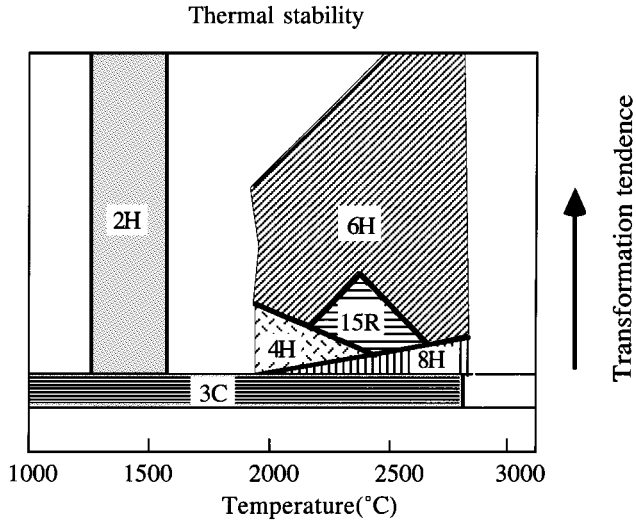

Figure 1 Polytype–temperature relationship of SiC, with a reference to Knippenberg [26]. The arrow denotes the order of transformation tendency from 3C to the other forms at various temperatures. The shadows stand for the relative amounts of different polytypes.

was performed at temperatures of 600–1500 K and at pressures of 5–25 GPa. The main purpose of our experiments was to investigate the shock effect and the binary effects of temperature and pressure on polytype transformation.

2. Experimental process

2.1. Experimental material

The starting materials (α-SiC and β-SiC) were ultrafine powders prepared by the chemical vapor deposition method. Their properties are summarized in Table I. The X-ray powder pattern of the β-SiC powder is shown in Fig. 2, and no peak for other polytype modifications was observed.

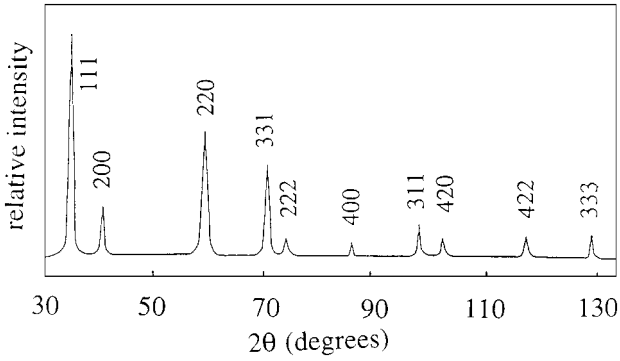

Figure 2 XRD pattern of β-SiC starting material used in the present study. All the peaks are identified as 3C-type SiC.

2.2. Shock recovery system

The powder was pressed into a SUS304 stainless-steel container. The outer dimension of the container was 24 mm in diameter × 30 mm in length and the inner space for the pressed sample was 12 mm in diameter × 2 mm in length. We applied an appropriate pressure ranging from less than 100 MPa to 600 MPa and obtained sample densities ranging from 1.5 to 2.4 g/cm^3, which were determined by their final volume and mass measurements.

Shock wave recovery experiments were carried out by using a 30 mm bore single-stage propellant gun. The projectile velocity ranged from 1 to 2 km/s, which was measured by flying magnet method. The assembly of the recovery system has been described elsewhere [17]. Besides the SUS304 stainless steel, we employed tungsten flyers to obtain higher pressure.

2.3. Shock pressure and temperature determination

The shock pressure for the SiC sample was estimated from the measured projectile velocity, using the impedance match method and the free surface velocity approximation. The Hugoniot equation of the state of SiC we used is:

$$Us = 3.0 + 1.5\,Up$$

when the initial density of the sample was close to 2.3 g/cm^3 [18]. The actual shock pressure might have been raised by multiple shock reflection. The shock temperature calculation was based on the following well-known equations, which referred to the isentrope [19],

$$dE = TdS–PdV \tag{1}$$

$$TdS = dE + PdV = Cv\,dT + CvT(\gamma/V)\,dV \tag{2}$$

$$dE = 1/2[(V_0 - V)\,dP - (P + P_0)\,dV] \tag{3}$$

$$E - E_0 = 1/2(P + P_0)(V_0 + V) \tag{4}$$

$$dT = (V_0 - V)/2Cv\,dP + [(P - P_0)/2Cv - T(\gamma/V)]\,dV \tag{5}$$

In our calculation, we chose the bulk modules B_0 and their pressure derivative $B_{0'}$ as 248 GPa and 4.0, respectively, for both β-SiC and α-SiC, which were obtained under static pressure up to 25 GPa [7]. For the Grüneisen parameter γ and the specific heat Cv, we used 1.2 and 0.71 × 10^{-3} KJ/g·K [10, 20], respectively. It should be noted that this calculated temperature is the average one for the powder sample. The grain surface may reach much higher temperatures than the inner part. Tables II and III list the experimental conditions employed in the study.

2.4. Post-shock sample treatment and examination method

The post-shock samples were removed by mechanically cutting the recovered containers using a lathe machine.

TABLE II A summary of experimental conditions and experimental results for α-SiC

#Run No.	ρ_0 (g/cm^3)	Vimp (km/s)	P_{1st} (GPa)	Temp. (K)	Estimated concentration (%) α-SiC 15R	6H	4H	β-SiC 3C	Δd (mm)/ε (%)	Powder size (nm)
α-SiC					15	75	6	4	—	400
#516	1.54	1.542	9.8	770	40	48	6	6	2.0/16.6	23
#514	2.05	1.525	12.1	710	37	52	7	4	1.1/9.2	23
#519	2.20	1.60	13.5	740	40	47	7	6	0.95/7.9	24
#515	2.09	1.786	15.1	890	38	48	8	6	1.3/10.8	20
#512	2.27	1.832	16.6	840	35	53	6	6	1.5/12.5	23
#511	2.28	2.039	19.3	1080	44	36	9	11	—	26
#520	2.20	1.746w	21.8	1260	49	31	8	12	4.1/34.2	32
#513	2.38	1.864w	25.1	1360	31	55	4	10	4.3/35.8	27

*denotes the starting material.
w stands for that shocked by a tungsten flyer.
d(mm) is the measured diameter change of the samples before and after shock loading.

TABLE III Part of the X-ray examination results of the post-shock β-SiC samples, with a comparison to 21R- and 33R-SiC

β-SiC d(nm)/In	Post-shock (#521) d(nm)/In	Post-shock (#510) d(nm)/In(%)	Post-shock (#517) d(nm)/In(%)	21R-SiC† d(nm)/In(%)	(h k l)	33R-SiC‡ d(nm)/In(%)	(h k l)
0.2519	0.2519	0.2519/100	0.2519/100	0.2518/100		0.2518/100	
				0.2515		0.2515	
				0.2473/20		0.2461	
						0.2433	
				0.2381/10		0.2373/60	
				0.2332		0.2341	
						0.2277	
	0.2279/w	0.2225/4		0.2231/10	1 0 13	0.2245/5*	0 1 20
0.2179	0.2179	0.2179/9	0.2184/9	0.2178/10	0 1 14	0.2178/30	1 0 22
	0.2088/s	0.2088/2	0.209/47	0.2075/8*	1 0 16	0.209/20	1 0 25
	0.2013/w	0.2013/5	0.203/9	0.201/30	0 1 17	0.2048/5*	0 1 26
	0.2000/m		0.200/9				
	0.1984/m	0.1951/2	0.198/25			0.1982/6*	1 0 28
	0.194/w			0.1926/2*	1 0 19	0.1952/2*	1 0 29
	0.1886/w		0.189/11	0.1878/1*	0 1 20		
				0.1742		0.1691/20	
0.1541	0.1541	0.1541/40	0.1541	0.1541/80		0.1541/80	

*denotes the calculated d values based on the single-crystal data of β-SiC in which a = 0.308 nm, $Cn = 0.252 \times n$ nm [14]. For 21R† with a reference to PDF 22-1319, while 33R ‡ to PDF 22-1316 · d values (nm) and their relative intensities (%) are also listed as d(nm)/In(%). In the second column, the relative intensities are indicated as strong (s), medium (m), and weak (w), respectively.
Experimental conditions: #521: P = 19.3 GPa, T = 1070 K; #510: P = 16.9 GPa T = 1020 K; and #517: P = 4.75 GPa, T = 920 K, respectively.

After cleaning in acetone, the samples were then immersed in a mixed acid solution (2HCl + HNO_3 mixed acid) for more than 24 h to decompose and to remove the metallic impurity. The undissolved portions were investigated by XRD, after simply grinding the sample into fine particles with an agate mortar. During X-ray examination, we applied Cu$K\alpha$ radiation, with a counter speed of 0.25°/min. Following Ruska's method [16], we obtained the contents of the four most common different polytypes of SiC. Using the Scherrer's equation [21], the average particle sizes were approximately obtained for both starting materials and post-shock samples, as referred to the starting SiC with an error less than 10%. They are listed in Table II.

In addition, the overall strain of the post-shock samples, ε, was defined as the radial change before and after shock along the direction normal to the shock wave propagation direction. It was estimated from direct dimensional measurement of the sample diameter in a container, as listed in Table II.

3. Experimental results

3.1. Polytype transformation from α-SiC

The experimental results on α-SiC are listed in Table II. It can be easily seen that the amount of α-type polytypes tends to decrease with the increase of shock temperatures. Conversely, a small amount of 3C-SiC polytype is found to increase slightly. These polytype phase transitions can be found based mainly on the change of 15R- and 6H-SiC. It is quite difficult to find an obvious change of 4H-SiC.

Fig. 3a, b, and c illustrate the relationship between shock temperatures and the estimated contents of 15R-, 6H-, and 3C-SiC polytypes, respectively. One can find from Fig. 3a that the amount of 15R-SiC polytype

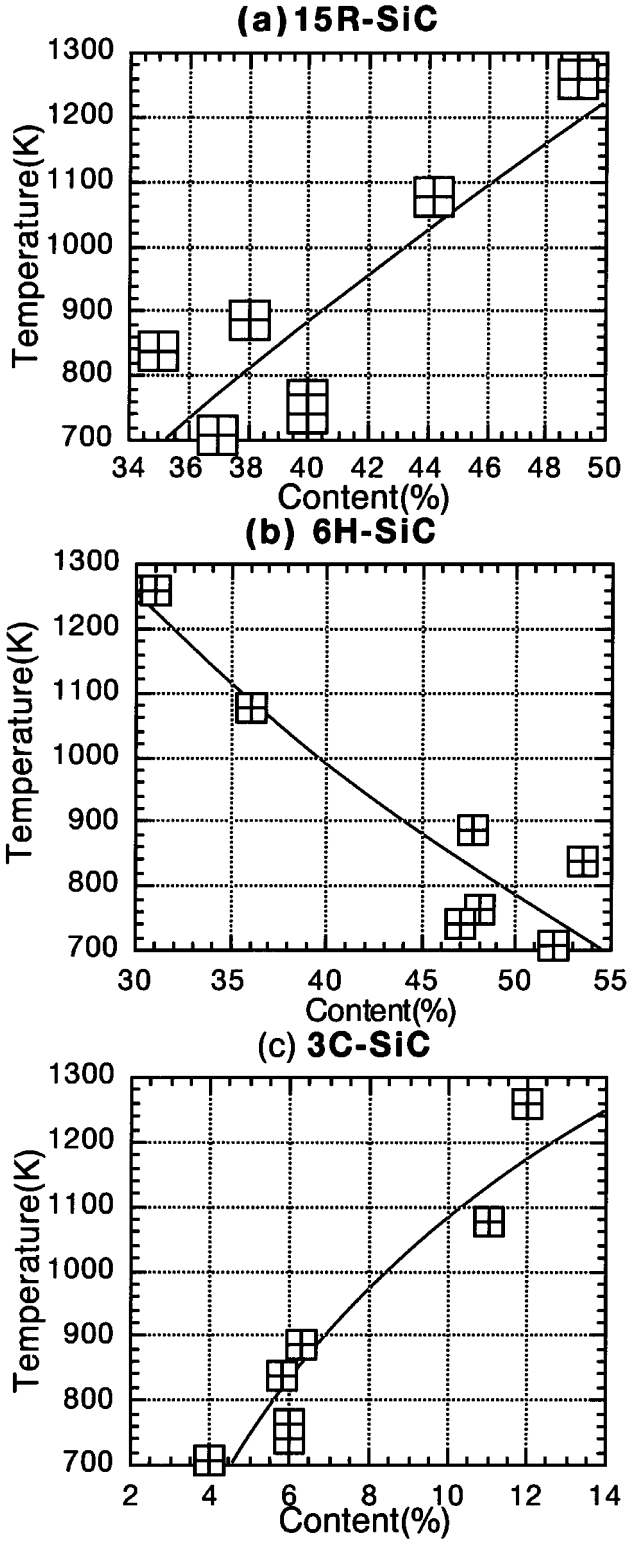

Figure 3 Estimated polytype content of 15R (a), 6H (b), and 3C (c) in post-shock samples from α-SiC, against the calculated shock temperatures.

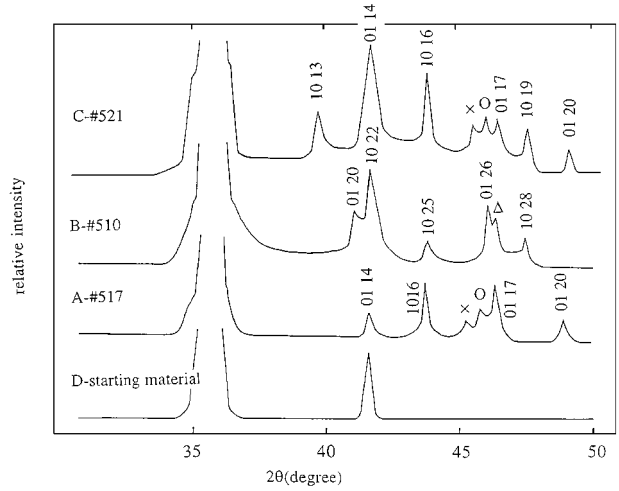

Figure 4 A series of XRD patterns observed in the post-shock samples from β-SiC. The new peaks can be indexed as 21R and 33R. O stands for (0 1 26) of 33R, and Δ for (0 1 17) of 21R. $\times$ is unidentified peak, was supposed to be a spit of the main peak.

increases gradually to about 50% for run #520 (the highest point) with the increase of temperature. Compared to the content of 15R in the starting material, a significant increase took place. In the range of the experimental conditions, 600∼1500 K, an increase of about 15% was identified. The contents of 6H-SiC decreased sharply from the initial 80% to 30%, through 50%, depending on the shock temperature. In the range of 600∼1500 K, a decrease of more than 25% was recognized. By a comparison with those of the above 15R and 6H polytypes, the 3C-SiC content-shock temperature relationship was comparatively steady (Fig. 3c). Within the present experimental conditions, the 3C-SiC content rose slightly with increasing temperature, and the increase almost equalled the difference between the decreases in 6H and the increases in 15R.

3.2. Rhombohedral phases from β-SiC

Experimental conditions for β-SiC are noted in Table III. Fig. 4 outlines typical parts of the XRD pattern for both the starting material and the post-shock samples from runs #510, #517, and #521. XRD results of the post-shock samples indicate the formation of new phases. The XRD analyses are summarized in Table III, together with some calculated d-spacing values and their comparative intensities (I) of SiC polytypes. Indexing the new peaks on the basis of the JCPDS cards, we find that they correspond to none of the d-value of hexagonal SiC (Set Nos. 29-1130, 29-1131, 22-1317, 22-1127, 22-1128) but of rhombohedral SiC; i.e., run #510 corresponds mainly to 21R, run #521 and #517 correspond mostly to 33R in terms not only of the d-values but also of the diffraction intensities [14]. In addition, we may notice that the post-shock products are a mixture of 21R and 33R, from the small peaks identified in Fig. 4. These data can support the finding that the new phases did appear after shock treatment of β-SiC, although they were only in small amounts ($< 5\%$).

4. Discussion

From the above experimental results, we consider that rhombohedral modification is the favored form for SiC under shock compression. In the literature, there were many reports about SiC polytypes under static high-pressure or nearly isothermal conditions at high temperatures [11]. Kondo *et al.* [13] performed a series of experiments on β-SiC under similar shock conditions, although they reported no phase change for β-SiC. It

is noted that the starting materials we employed in this study were very pure; thus, the effects of impurities on the phase transitions could be negligible.

4.1. Nature of shock compression

Before further discussion, it is valuable for us to review the typical nature of the shock wave we used in this study. The conceptual thinking of our shock compression induced by planar impact as an idealized one-dimensional model is acceptable, although its actual nature of a shock wave profile in solids, especially for porous powders, is very complex. Due to the passage of a shock wave in a powder assemblage, not only high pressure but also high temperature may be generated adiabatically within a very short time duration, normally less than 100 nano-seconds. It is believed that non-uniform higher temperature distribution can take place on the surface of the particles or voids due to intense heating under shock compression. Sometimes the releasing process from the extremely high temperature will have a great influence on the samples, namely an annealing effect. The impacts will cause structural defects in solids, such as lattice defects, dislocations and/or stacking defaults, particle size reduction, and even phase transitions. These effects are remarkable in inorganic materials having ionic and covalent chemical bonding, and they are thought to be caused mainly behind the shock wave front [13]. The high pressures generated by the shock wave were sometimes seen as analagous to that of the hydrostatic pressure, however this referred only to the average one and the macroscopic effects. Actually, the final shock pressures in local grains can be much higher than the average one attained at steady state. This also applies to the temperature. These natures should have great effects on our samples during every step treatment.

4.2. Shock pressure effect on α-SiC

For α-SiC starting material, its initial polytype content was determined as 6H : 78%, 15R : 15%, 4H : 7% and 3C : 4%; clearly, it mainly consists of 6H- and 15R-SiC. Considering our sample assemblages, their densities varied from 1.5 g/cm^3 to 2.4 g/cm^3 (see Table II), which were typical porous materials to the single-crystal density of 3.2 g/cm^3 for SiC. Under shock conditions, all the effects mentioned above would act on these samples.

With a pressure loading, materials will turn to reduce its volume and change to high-density modifications. For 6H-SiC, its atom layer stacking sequences within a unit cell are: A B C A C B . . . , according to the classical *ABC* atom stacking sequence, and it belongs to simple packed hexagonal lattice structure. With the action of hydrostatic pressure, 3C SiC transforms to its high-density form, rock salt form [11], and 6H-SiC also transferred to its high-pressure phase above 105 GPa by shock compression [12]. The pressure of the porous powders generated by shock loading in this study was much lower than these pressure ranges. The polytype transitions in our experimental results might suggest some obvious differences of the shock loading from hydrostatic loading. Also, the temperature effects on these transformations should not be ignored.

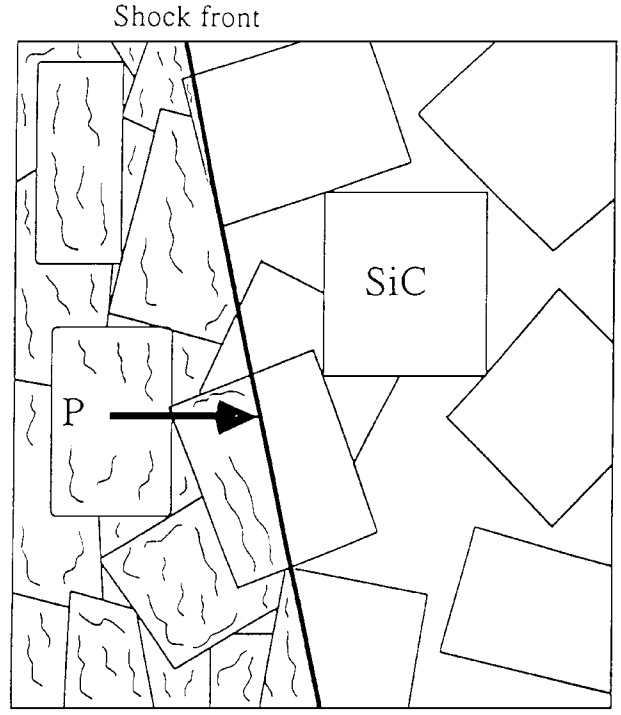

Figure 5 Schematic representation of SiC powders as cubic particles stacked in a simple arrangement. It also shows the action of one-dimensional shear stresses on the particles caused by the shock wave. A heavy line indicates the shock front moving to the right. The arrow P denotes the shock pressure. The shocked part is associated with particle fracture and stacking sequence change.

It is true that the particle size reduction resulted from the shock loading and the powder movement in the shock front [13, 22] with as greater tendency for larger particles to undergo fracture while smaller ones plastically deform, which was previously reported by Potter and Ahrens [23] for diamond powders. In our starting α-SiC material, the average particle was of nano-meter size. Thus, we found a dimensional reduction on average, thereby implying a series of lattice distortion or stacking sequence changes at the same time. From the measured deformation and the reduction in particle size listed in Table II, one can confirm the stress effects and the powder deformation. This evidenced the effect of shock pressure on these plytype transitions. Fig. 5 illustrates the kinds of shear stresses acting on the particles and clearly shows how they took place just behind the shock front. Besides the reduction of particles size by these one-dimensional shear stresses, some atom layers might move and change to other stacking positions. It is clear that the transition from hexagonal type to rhombohedral type involves almost no density change, which implies that the transition does not require much energy. The energy refers to either high pressure or high temperature, or both. It is supposed to be a significantly important contribution to the decreases of 6H-SiC and increases of 15R-SiC along with increasing the shock pressure. It is obvious that if higher shock pressure is applied, higher shear stress might occur and more stacking defects or phase transition would be favored to happen. We now discuss the effect of shock temperature.

4.3. Shock temperature effect on α-SiC

The effects of temperature on polytype transformation are summarized in Fig. 1 at 1 atm. The 6H- and 15R-SiC were believed to be the modifications above 2000 K. In our experimental conditions (see Table II), the highest shock temperature was significantly below this scale, which implies that the temperature effect may have little significance in driving polytype transformation. However, our experimental results show some important influences on the polytype transformation in the recovered samples, subject to the calculated shock temperatures of 600∼1500 K. We consider that the heterogeneous temperature increases in the powder samples, especially on the surface of the grain, may activate some of the gliding planes of the crystals during shock compression.

From the experimental results (Table II), initial densities also indicate an important impact on the polytype transformation. For run #513, the initial density of the sample was the highest, subjected to the highest pressure and temperature. In run #516, with the lowest density, the transformation yield from 6H- to 15R-SiC was slightly higher than that in run #514. This may indicate that a lower density caused higher heterogeneous temperature distribution, while a higher density produced relatively uniform temperature distribution. The extent of temperature heterogeneity may control the yield of phase transition rather than the pressure effect. Therefore, even if run #513 had the highest average shock pressure and temperature, the transformation yield was still comparatively lower. This analysis may lead to the idea that these polytype transitions depend not only on the calculated average pressure and temperature but also on the uniformity of pressure and temperature in each grain, which relies on the initial density or void volume before shock compression. Although with the same densities, the increase of either pressure or temperature enhances the transformation, the effect of temperature is much stronger than that of pressure.

4.4. Polytype transformation of β-SiC

In the samples recovered from β-SiC, the new peaks in XRD patterns were observed corresponding to the rhombohedral phases. These rhombohedral phases possess relatively longer periods while hexagonal types (2H, 4H, 6H, 8H) are of shorter durations. In Fig. 4, the new peaks are identified mainly as 21R for run #510 and 33R for runs #521 and #517. However, the peaks around 45° of 2θ strongly suggest they correspond to mixtures of 21R and 33R, and they are dominated according to different experimental conditions. In Sections 4.1 and 4.2, the effect of heterogeneous shear stress and non-uniform temperature on the polytype transformation of α-SiC are also compared to that of β-SiC. Thus, under these deviatoric stresses the post-shock products consist of one main phase and a small part of another. In run #517, its initial porosity was the highest; therefore, even if the average shock temperature was estimated to be lower, its local temperature was probably still as high as in run #521. This is why the recovered sample of run #510 was different than those of runs #521 and #517 in terms of the dominant products. After examining the *d*-values corresponding to the new peaks in Table III, one can easily recognize the similar stacking sequences and the occurrence of stacking defaults out of cubic SiC, (1 0 16), (1 0 17), (1 0 25), (1 0 26), (1 0 29), (1 0 30) and so on. They may have resulted from one-dimensional pressures or stresses. In β-SiC crystal structure, the close-packed atom layer is {1 1 1} planes, and in α-type SiC crystals, it corresponds to {0 0 0 1} planes. Under one-dimensional shock load or shear stress, the movement of the close-packed atom layer {1 1 1} occurred, therefore these new crystal planes appeared. During the phase transition, rhombohedral structures contained much more "disordered" stacking than those of hexagonal ones, which might be why the final products were rhombohedral SiC instead of hexagonal SiC. It is noted that the heterogeneous stress distribution on local grains determined the structures of product phase, i.e., 21R, with the Zhdanov symbol [24] of $(34)_3$ structure, or 33R, with $(3332)_3$ structure. The structures with a comparatively longer period are preferred in the post-shock samples because of the higher "disorder" level.

The different results between Kondo *et al.*'s consolidification study and this report, even under almost the same shock conditions, are mainly due to the powder size differences. In their study, the average particle size was 0.28 μm, nearly ten times larger than ours. More fractures happened to the larger particles; more energies are absorbed by these fractures and thus less energies are available on phase change.

4.5. Stacking sequences change resulting in polytype transitions

One question that arises is how these stacking sequences changed by shock compression, i.e., what was the mechanism of transformations among these polytypes? To investigate these transitions, let us first note their standard stacking sequences. The stacking sequences are described as A B C A C B $\cdots$ for 6H, A B C $\cdots$ for 3C, and A B C B A C A B A C B C A C B $\cdots$ for 15R. With shock loading and shear stress, these atoms would change to the other stacking positions. In a model established by Horie and Sawaoka [19] illustrating the reaction of crystal structures among hexagonal graphite, rhombohedral graphite, and cubic diamond, the effects of the shock wave on these transitions could be clearly seen. We can interpret the mechanism of these transitions among SiC polytypes the same way as the transformation from *hp* graphite to *fcc* diamond, but we ignore the very trace effect of lattice-spacing change in SiC. Following this model, the stacking sequence change from 6H to 15R may be described as following:

6H: A B C A C B A B C A C B A B C

15R: A B C <u>B A C</u> A B <u>A C</u> <u>B C</u> A C B

The underlined symbols in 15R denote the layers performing the change. Fig. 6 clearly illustrates the movement process of the atom layers in this transformation by a zigzag sequence model, from

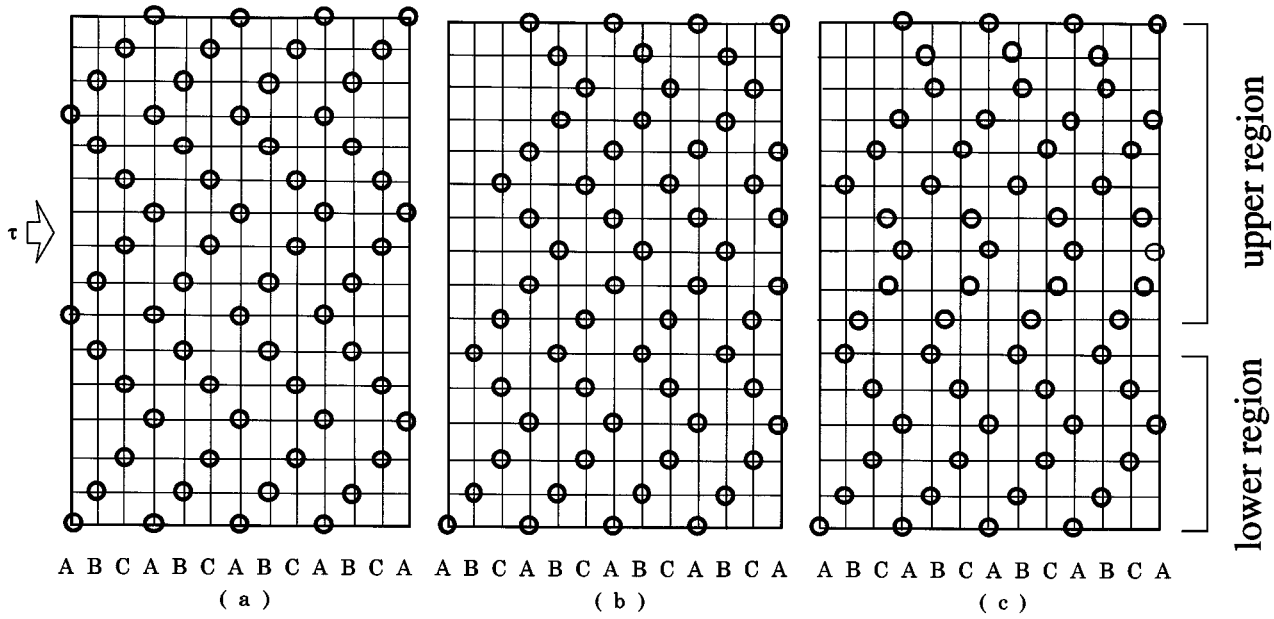

Figure 6 (a, b, c). Zigzag sequence of SiC atoms in the (1 1 20) plane showing the stacking sequence changes from 6H type to 15R type under the heterogeneous shear stress, τ. Only the silicon atoms are shown in this description [25]. (a) 6H type; (b) intermediate period; and (c) is the final 15R type. Note that atoms in the upper region in (a) move to the right and that atoms in the lower region in (a) do not change their relative position in the course of transition of 6H to 15R.

which one can know how the atom layers change their stacking sequences by heterogeneous shear stresses. It should need little energy or pressure and should be comparatively easier than the following stage:

$$\text{15R: A B C B A C A B A C B C A C B} \cdots$$

$$\text{3C: A B C } \underline{\text{A B}} \text{ C A B } \underline{\text{C A}} \text{ B C A } \underline{\text{B C}} \cdots$$

while accompanying more ordered crystal lattice structure appeared. It is thought to be similar for β-SiC starting materials being transferred to 21R- or 33R-SiC under this non-uniform shock loading, from short-period stacking to longer ones. It depends on the actual local conditions for final products to be recognized as 21R- or 33R-SiC polytype.

Therefore, the above polytype transitions for both α-and β-type starting materials involve only the exchange of stacking sequence of atoms. The stacking sequences transposition by shock wave results in these polytype transformations. In the present study, taking into account the short time duration of the shock wave and the lower shock temperature, we consider that diffusion-induced phase transition hardly happened. This stacking sequence change of atoms can be regarded as atomic layer transposition, in the solid state. It is similar to that of the phase change of SiC at high temperatures [25]. For β-SiC, transformation mechanisms in the solid state are not known [26].

On the basis of the above experimental results and analysis, it is believed that all the above changes are diffusionless phase transitions and follow the layer-transposition mechanism [25].

5. Summary

Under the shock conditions applied in this study, polytype transitions occurred from both α-SiC and β-SiC starting materials, which indicate significant differences than those studies under static high-pressure and high-temperature. Many factors control these transitions, such as particle size and initial density of the starting materials, as well as shock pressure and shock temperature. However, the non-uniform distribution of shock temperature and the heterogeneity of one-dimensional stress play important roles. From our results, rhombohedral modifications are the favored occurrences under the shock conditions of 600–1500 K and 5–25 GPa. The possible mechanism for these phase transitions is the stacking position changes of atoms within close-packed atom layer by one-dimensional stress. The shear stress as well as the heterogeneity of stress in shock-loaded powders helps the stacking position change. It follows the layer-transposition mechanism.

Acknowledgements

The authors would like to thank Sumitomo Osaka Cement Co. for kindly providing both SiC starting materials. We thank Mr. T. Osawa for his experimental help.

References

1. M. G. SPENCER, *et al.* "Proceedings of the Fifth Conference on Silicon Carbide and Related Materials," IOP Conf. Proc, No. 137 (Institute of Physics and Physical Society, Bristol, 1994) p. 1.
2. A. ADDAMIANO, in "Silicon Carbide–1973," edited by R. C. Marshal, J. W. Faust, Jr., and C. E. Ryan (University of South Carolina, Columbia, 1974) p. 179.
3. Z. INOUE and Y. INOMATA, *J. Crystal Growth* **50** (1980) 779.
4. H. N. BAUMANN, Jr., *Electro-Chem. Soc.* **99** (1952) 109.
5. W. F. KNIPPENBERG and G. VERSPUI, *Mat. Res. Bull.* (Special Issue) **4** (1969) 44.
6. E. D. WHITNEY and P. T. B. SHAFFFER, *High Temperatures–High Pressures* **1** (1969) 107.

7. K. STRÖSSNER, M. CARDONA, and W. J. CHOYKE, *Sol. State Comm.* **63** (1987) 113.
8. A. F. GONCHAROV, E. V. YAKOVENKO, and S. M. STISHOV, *JETP Lett.* **52** (1990) 9491.
9. S. SHINOZOKI, R. M. WILLIAMS, B. N. JUTERBOCK, W. T. DONLON, J. HANGAS, and C. R. PETERS, *ACS Ceramic Bull.* **64** (1985) 1389.
10. J. LIU and Y. K. VOHRA, *Phys. Rev. Lett.* **72** (1994) 4105.
11. M. YOSHIDA, A. ONODERA, M. UENO, K. TAKEMURA, and O. SHIMOPMURA, *Phys. Rev.* **B48** (1993) 10587.
12. T. SEKINE and T. KOBAYASHI, *ibid.* **B55** (1997) 8034.
13. K. KONDO, S. SOGA, A. SAWAOKA, and W. ARAKI, *J. Mater. Sci.* **20** (1985) 1033.
14. H. JAGODZINSKI and H. ARNOLD, in "Silicon Carbide," edited by J. R. O'Connor and J. Smiltents (Pergamon Press, New York, 1960) p. 136.
15. L. K. FREVEL, D. R. PETERSEN, and C. K. SAHA, *J. Mater. Sci.* **27** (1992) 1913.
16. J. RUSKA, L. J. GAUCKLER, J. LORENZ, and H. U. REXER, *ibid.* **14** (1979) 2013.
17. T. SEKINE, M. AKAISHI, N. SETAKA, and K. KONDO, *ibid.* **22** (1987) 3615.
18. S. P. MARSH (ed), "LASL Shock Hugoniot Data" (University of California, Berkeley, 1980) p. 329.
19. Y. HORIE and A. B. SAWAOKA, "Shock Compression Chemistry of Materials" (KTK Scientific Publisher, Tokyo, 1993) p. 283.
20. M. NEUBERGER, *Mater. Res. Bull.* (Special Issue) **4** (1969) 365.
21. B. E. WARREN, "X-Ray Diffraction" (Addison-Wesley Publishing Company, Inc, Massachusetts, 1969) p. 253.
22. S. S. SHANG and M. A. MEYERS, *J. Mater. Sci.* **31** (1996) 252.
23. D. K. POTTER and T. J. AHRENS, *Appl. Phys. Lett.* **51** (1987) 317.
24. G. S. ZHDANOV, *Compt. Rend. Acad. Sci., URSS* **48** (1945) 43.
25. H. JAGODZINSKI, *Acta Cryst.* **7** (1954) 300.
26. A. R. VERMA and P KRISHANA, "Polymorphism and Polytypism in Crystals" (John Wiley & Sons, Inc., New York, 1960) pp. 60, 266.
27. W. F. KNIPPENBERG, *Philips Res. Rept.* **18** (1963) 161.

Received 2 April 1997
and accepted 6 August 1998